Vibroacoustic optimization of electric motors taking advantages of viscoelastic resins

Emeline Sadoulet-Reboul[1], Kévin Jaboviste[1], Morvan Ouisse[2], Adrien Parpinel[3], Pascal Bouvet[3], Fabien Maugan[4], Christophe Espanet[4]

[1] *Université de Franche-Comté, CNRS, institut FEMTO-ST, F-25000 Besançon, France*

[2] *SUPMICROTECH, Université de Franche-Comté, CNRS, institut FEMTO-ST, F-25000 Besançon, France*

[3] *Vibratec, 28 Chemin du Petit Bois, 69130 Écully, France*

[4] *Moving Magnet Technologies, 1 Rue Christian Huygens, 25000 Besançon, France*

Abstract

Electric drivelines are the source of tonal noise which can be particularly unpleasant in many industrial settings, and in particular in vehicles. Different approaches are investigated to minimize this phenomenon, based on the control of the electromagnetic source for example, or on the optimization of the structural design. This paper introduces a framework allowing time-efficient reduction of noise radiation without affecting electromagnetic performance of electric motors, based on the combination of reduced order model and optimization of viscoelastic properties of potting resins. Although viscoelastic resins are frequently used in electric motors, they are primarily used for insulation, protection, and mechanical stability. The originality of this work is to endow them with a new functionality by dimensioning them in such a way as to reduce acoustic radiation. Indeed, the elastodynamic properties of resins depend on the frequency and on the temperature, and can be optimized to reduce the vibrations and thus the radiated noise. The design is complex because it involves coupled multiphysical phenomena that cannot be considered separately, and because the numerical models considered are large-scale models. A methodology is proposed in this paper and applied to the case of a high-speed electric motor. To guarantee fast and accurate estimation of the acoustic power in the optimization process, a reduced order model of the engine is developed from a multi-model basis taking into account the thermal and frequency dependencies of the materials. The numerical optimization thus carried out allows to identify the optimal resin properties, and a motor is coated to experimentally validate the results. Experimental characterization thus confirms that the radiated noise can be considerably reduced by using a suitable resin. This work opens the way to a new design strategy for electric motors providing resin coating with an acoustic function.

Keywords: `Electric motor, Vibroacoustics, Viscoelastic, Optimization, Reduced-Order Modeling`

1. Introduction

Electric motors are more and more used in the transport industry, identified as a green energy likely to help to meet the environmental requirements. The principle is based on the conversion of electrical energy to mechanical one, usually by employing electromagnetic phenomena. Compared to more conventional combustion engines, these devices have a specific acoustic signature, as the vibratory and noise come from a new physical source. In particular the noise emitted features both pure tonal components due to the magnetic field, and

*emeline.sadoulet-reboul@univ-fcomte.fr

modulated high-frequency tones due to the Pulsed Width Modulation. Studies show that an increasing level of these high frequency tonal components leads to a feeling of aggressiveness, powerful and unpleasantness [**?**]. It is thus important to take these specific phenomena into account for design purposes. The mechanism of noise emission is quite well-known: the phase current in the stator coil generates time-varying Maxwell forces in the air gap between the stator and the rotor poles, these forces induce vibrations that propagate in the structure of the stator, and are radiated. The prediction of the vibroacoustic behavior thus require to use adequate multiphysic tools to capture all the physical phenomena. Classically, the excitation is computed thanks to an electromagnetic simulation on a 2D Finite Element Model of a stator cross-section, then the forces on the electromagnetic mesh are projected on a 3D structural Finite Element Model of the stator. The vibratory response is then computed based on the modal superposition method, and finally the noise radiated is computed using the Finite Element Method, the Boundary Element Method or an analytic estimation of the Equivalent Radiated Power (ERP) level. The methodology has given rise on a huge literature where the approach is applied to permanent magnet synchronous motor (PMSM) [**? ? ? ? ? ?**], on a wound-rotor synchronous machine [**?**], or on a Switched-Reluctance Motor [**?**], among others. Models are of increasing complexity, taking into account the anisotropy of the stator [**? ? ? ?**], the non-uniformly distribution of electromagnetic forces or the effect of the windings [**?**]. Despite the maturity of the global simulation process, computation times are huge as it implies the use of large structural Finite Element Models: reducing vibration and noise using optimization studies then becomes prohibitive with regard to the calculation time required to carry them out. Nevertheless the approach is feasible and has been applied to investigate optimal configurations for intrinsic properties of the structure or for electromagnetic forces. For instance, in [**?**], two parameters of the rotor shape, the claw angle and the trailing edge size are optimized to reduce noise of a claw-pole alternator. In the case of a PMSM, [**?**] proposes an optimization configuration for the slot opening width, the pole arc ratio, the magnet shape and the stator yoke thickness ; an optimization strategy of rotor slot fit is also proposed in [**?**]. [**?**] shows that magnet skewing is a better solution to reduce the noise over a wide frequency band than optimizing slot opening width and magnet shape form ; optimization of V-shaped skewed slots for noise reduction is also investigated in [**?**]. [**?**] performs an optimization on five geometric parameters, [**?**] obtains a high noise level reduction on a wide speed range with small changes on the shape of the rotor poles, and investigates the impact of uncertainties. Another approach is investigated in [**?**] where topology optimization based on element density as a design factor is used to redesign two shapes of a motor housing to reduce vibrations. Quantities at the heart of all these optimization studies are geometric parameters.

This paper investigates a new paradigm by considering the embedding resins introduced in electric motors as endowed with functional properties for vibroacoustic control, and proposes a complete methodology for optimizing the complex multiphysics problem induced by their design. These resins are mainly used to protect fragile or exposed components and for thermal management, but they also present a viscoelastic behavior likely to be interesting for vibration reduction, and little or not exploited. Indeed, viscoelastic materials present high damping capacities in some temperature and frequency ranges: by comparing 12 resins with different viscoelastic properties [**?**] has shown that a reduction of peak equivalent radiated power values of 5 to 10 dB could be achieved. One of the difficulties of implementation in this comparison approach is related to the computation time required to solve each study case by the Finite Element Method, such that a global

optimizaton study on the characteristic behavioral parameters of a resin is too time-consuming for industrial applications. To undergo this problem, a structural model reduction strategy adapted to the study of electric motors incorporating viscoelastic resins is presented in this paper: the method is based on a multi-model reduction that allows to take into account the vibrations in the dynamic behavior of a structure as a function of parameters such as frequency and temperature. The method provides the optimal resin parameters. The resulting selected resin has been implemented on the real motor to perform the experimental validation. The paper is organized as follows: the equations used to compute the noise radiated by an electric motor working with a Finite Element model are detailed in section 2. The vibroacoustic problem implying a full-scale model of an electric motor is detailed in section 3, based on an adapted multi-model reduction strategy. Finally, results given by the optimization process are presented in section 4, and they are validated by comparison with experimental results in section 5. The work was carried out in collaboration between FEMTO-ST research institute, Vibratec company, expert in acoustic and vibration control, Moving Magnet Technologies (MMT) company, expert in the design of electromagnetic solutions, in the framework of the FUI e-Silence project dedicated to the Silent design of electrical machines.

2. Multiphysics computation of the radiated noise

This section details the global approach to solve a vibro-acoustic problem for the case of an electric motor. The methodology is applied on a patented high speed motor with 6 coils and 4 poles developed by MMT [**?**] for a supercharger (see Fig.1). Fig. 2 shows the overall process used to compute the noise radiated by the

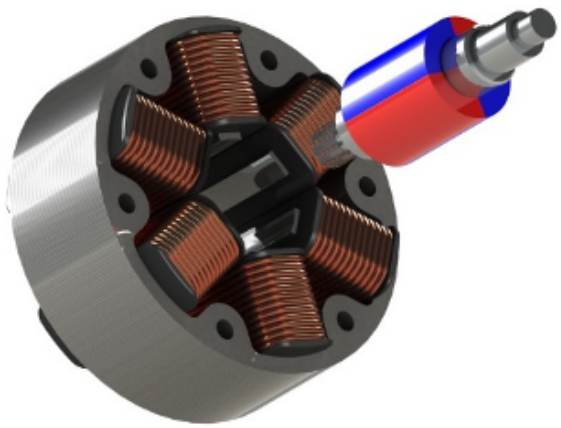

Fig. 1: View of the electric motor (Moving Magnet Technologies)

motor. An electric current feeds the windings mounted on the stator teeth to generate an electromagnetic flux, and thus to obtain a torque. In practice, the flux density is calculated at the motor's air gap, which makes it possible to obtain Maxwell's stresses. The projection of the Maxwell forces onto the tooth meshing [**?** **?**] is performed before the computation of the vibratory response of the electric motor. In the case of a motor with resin, the viscoelastic behavior of the resins must be taken into account in the calculation of the vibratory response: this question is investigated in detail in the next section. Finally, from the knowledge of the velocity

field on the skin of the stator, it is possible to calculate the Equivalent Radiated Power (ERP) by taking or not into account a radiation factor.

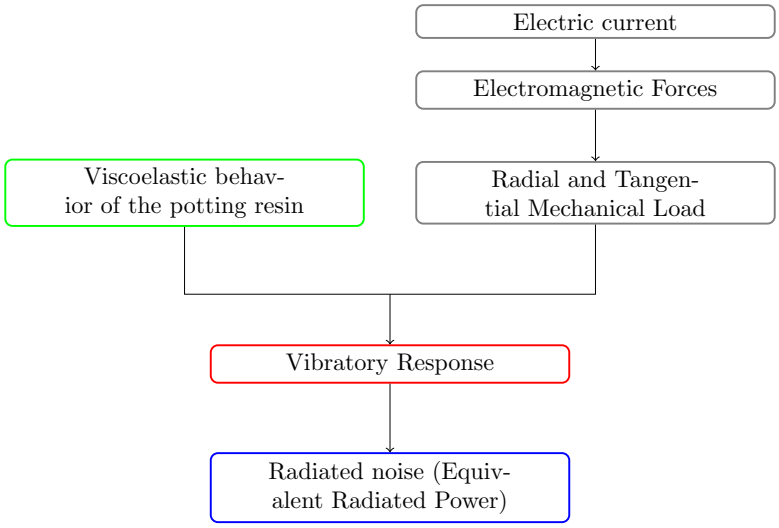

Fig. 2: Global process for the computation of the noise radiated by an electric motor.

For the considered study, the radial and tangential mechanical loads to be applied on the inner face of the stator teeth are input data provided by Vibratec from electromagnetic FLUX® simulations.

2.1. Finite Element Model of the motor and Dynamic Study

The dynamic behavior of the motor is computed by the Finite Element Method (FEM) implemented in the commercial software NASTRAN®. Fig. 3a shows the Finite Element Model for the studied electric motor. It is composed of a stator with a transverse orthotropic behavior updated from vibratory tests to represent the behavior of the stack of metal sheets, and of aluminium flanges [**?** **?**]. Fig. 3b shows the windings around the stator teeth, a contact interface skin is introduced to calibrate the numerical model based on experimental measurements. The three steel pins are also included in the model to obtain the rigidity experimentally observed. The model of the rotor is based on beam elements taking into account the stiffness provided by the ball bearings. The rest of the structure is meshed with quadratic tetrahedrons elements.

Regarding the boundary conditions applied to the Finite Element Model of the electric motor, it is considered to be free and a mechanical torque in radial and axial direction is applied on the inner face of the stator teeth. Free boundary conditions enable the analysis to proceed without needing to account for the actual integration conditions, which remain unknown, thereby simplifying the model and focusing on inherent structure behavior. The torque is representative of the 4^{th} engine order and results from the integration of Maxwell's efforts at the motor's air gap. This specific engine order is investigated as it leads to the highest radiated noise on the frequency band of interest because it directly excites the ovalization mode (2,0) of the stator (see Fig. 4). The dynamic equation governing the behavior of the electric motor without the potting resin is written in the frequency domain as

$$-\omega^2 \mathbf{M}\hat{\mathbf{U}} + (1 + j\eta_e)\mathbf{K}_e\hat{\mathbf{U}} = \hat{\mathbf{F}}_e, \tag{1}$$

where ω is the pulsation, $\mathbf{M}$ is the mass matrix of the whole electric motor, η_e is the structural damping[1], $\mathbf{K}_e$

[1]Without loss of generality, this expression assumes homogeneous structural losses. It easily extends to non-homogeneous

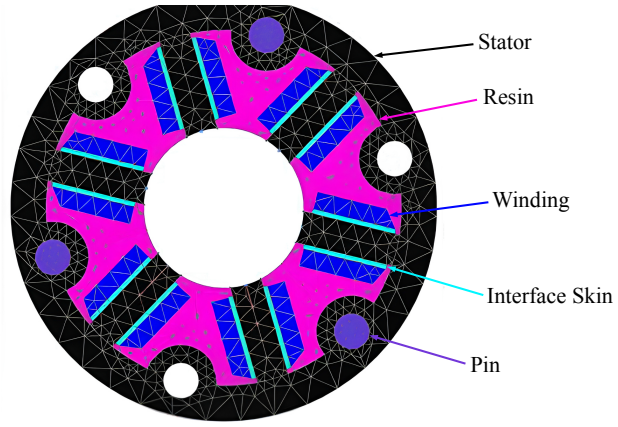

(a)

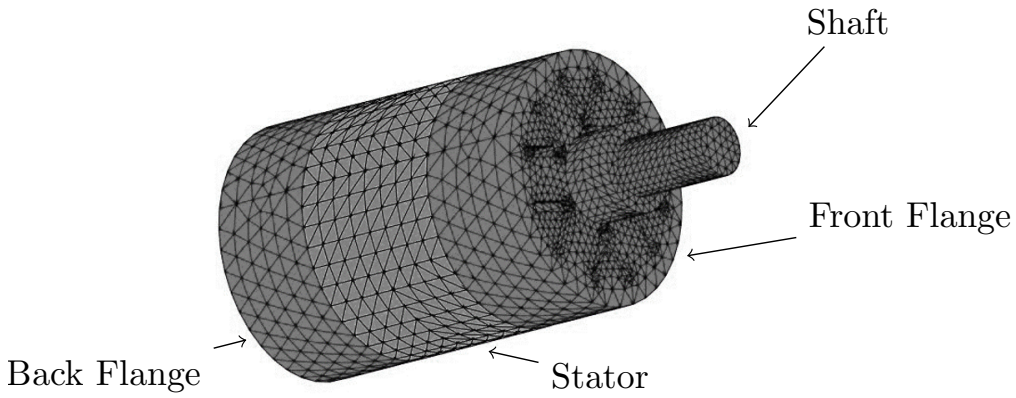

(b)

Fig. 3: (a) Finite Element Model of the electric motor, (b) 2D View: the coils are fixed on the teeth of the stator with an adhesive.

represents the stiffness matrix. $\hat{\mathbf{F}}_e$ is the mechanical load vector and $\hat{\mathbf{U}}$ is the displacement field vector. The velocity field required for the computation of the next step is deduced from the displacement field obtained by solving Eq. 1.

2.2. Acoustic computation

The Equivalent Radiated Power is first approximated from the velocity of elements located on the external surface of the stator:

$$ERP(\omega) = \frac{1}{2}\rho_{air}c_{air}\sum_{i\in skin} V_{i,n}^2(\omega)S_i, \tag{2}$$

where ρ_{air} is the air density, c_{air} is the speed of sound in air, $V_{i,n}$ is the averaged normal velocity of element i at frequency ω and S_i is the surface of element i belonging to the external surface *skin* of the stator. As the radiation efficiency is not constant over the frequency range of interest, the radiation factor $\sigma(\omega)$ (Fig. 5(a)) is introduced to compute the corrected Equivalent Radiated Power [**?**],

$$ERP^{\sigma}(\omega) = \sigma(\omega)ERP(\omega). \tag{3}$$

Fig. 5(b) shows the evolution of ERP^{σ} according to the frequency for the electric motor without potting

dissipation.

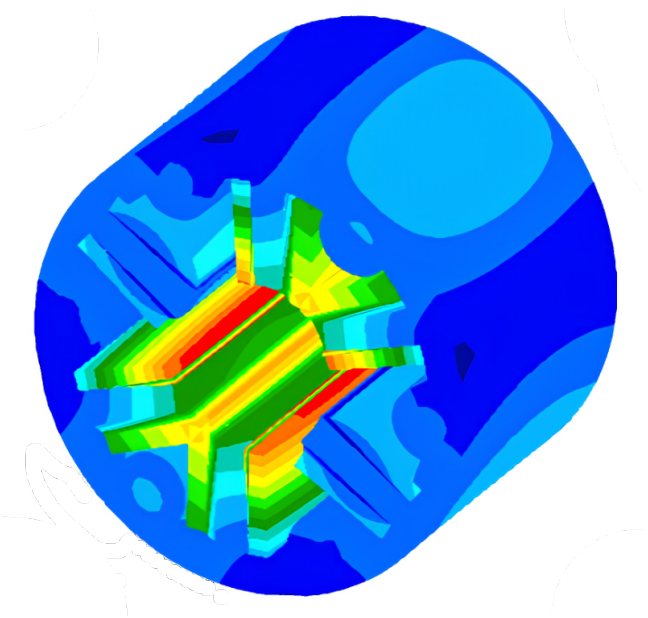

Fig. 4: Critical vibration mode on the frequency band of interest: Ovalization mode (2,0).

resin. This figure shows that the level of ERP exceeds 80 dB on two frequency ranges, around 4 kHz and 7 kHz. As expected, the ovalization mode (2,0) already mentioned is responsible for the first maximum observed close to 4 kHz. The contribution of this particular mode to the ERP around 7 kHz is however limited as the acoustic radiation in this range is mainly due to the eigenmode whose shape is shown in the figure. This latter is a priori less efficient in terms of acoustic radiation than the previous one, but the spatial distribution of the electromagnetic excitation combined with the shape of the mode and its radiation efficiency results in an overall high pressure level mainly due to this particular mode.

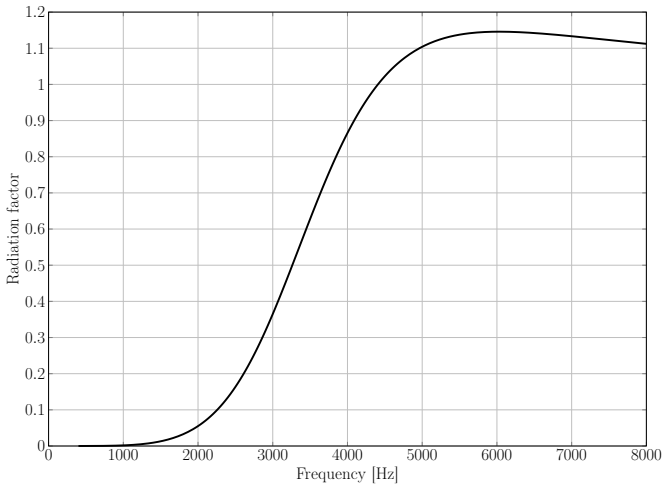

(a)

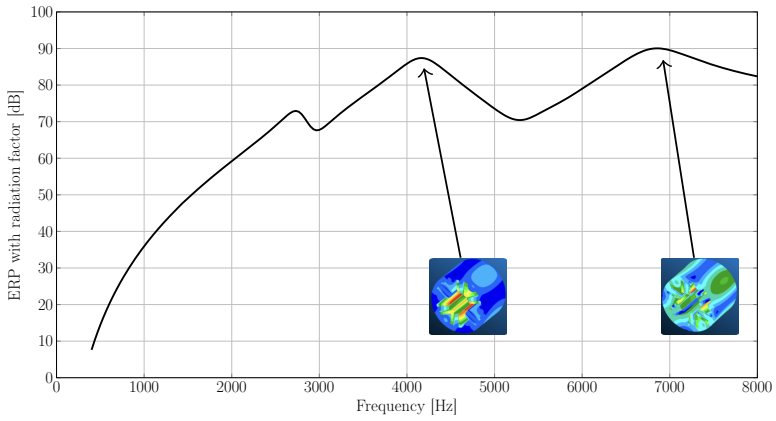

(b)

Fig. 5: Radiation factor σ evolution according to the frequency (a), ERP^{σ} of the motor without potting resin (b)

3. Optimization of electric motor vibroacoustics by tuning viscoelastic resins

Windings can be encapsulated (potted) or impregnated with viscoelastic resins. As an illustration, the windings of the motor considered here are embedded in a resin volume shown in magenta in Fig. 3b. In electric motors, resins are commonly used for electric insulation, thermal management, corrosion protection, chemical protection, and position holding. The new idea is to select them on the basis of their viscoelastic properties to minimize the radiated noise. An adapted rheological model is proposed to describe the viscoelastic behavior of the resins and introduced in the dynamic equations. The challenge is then to reduce computational times to allow the optimization study.

3.1. Dynamic behavior of the motor including viscoelastic resins

Taking into account the viscoelastic behavior of the potting resin, the dynamic equation of the electric motor in the frequency domain is written,

$$-\omega^2 \mathbf{M}\hat{\mathbf{U}} + (1 + j\eta_e)\mathbf{K}_e\hat{\mathbf{U}} + \mathbf{K}_Z(\omega, T)\hat{\mathbf{U}} = \hat{\mathbf{F}}_e, \tag{4}$$

where $\mathbf{K}_Z(\omega, T)$ is the frequency- and temperature-dependent stiffness matrix associated to the potting resin. It should be emphasized that, even if the notation is similar, the degrees of freedom differ from Eq. 1 as they include those of the resin. Also, the mass matrix includes here the inertial properties of the resin.

Four different potting resins are considered here on the basis of their thermal properties compatible with the requirements of the engine. They are referred as A, B, C and D. The resins are characterized on a Metravib DMA+ 300 viscoelastic machine providing the values of the storage modulus and loss factor over temperature (from -30 to 170 °C) and frequencies (from 1 to 31.5 Hz). Fig. 6 shows the evolution of these parameters for resin A.

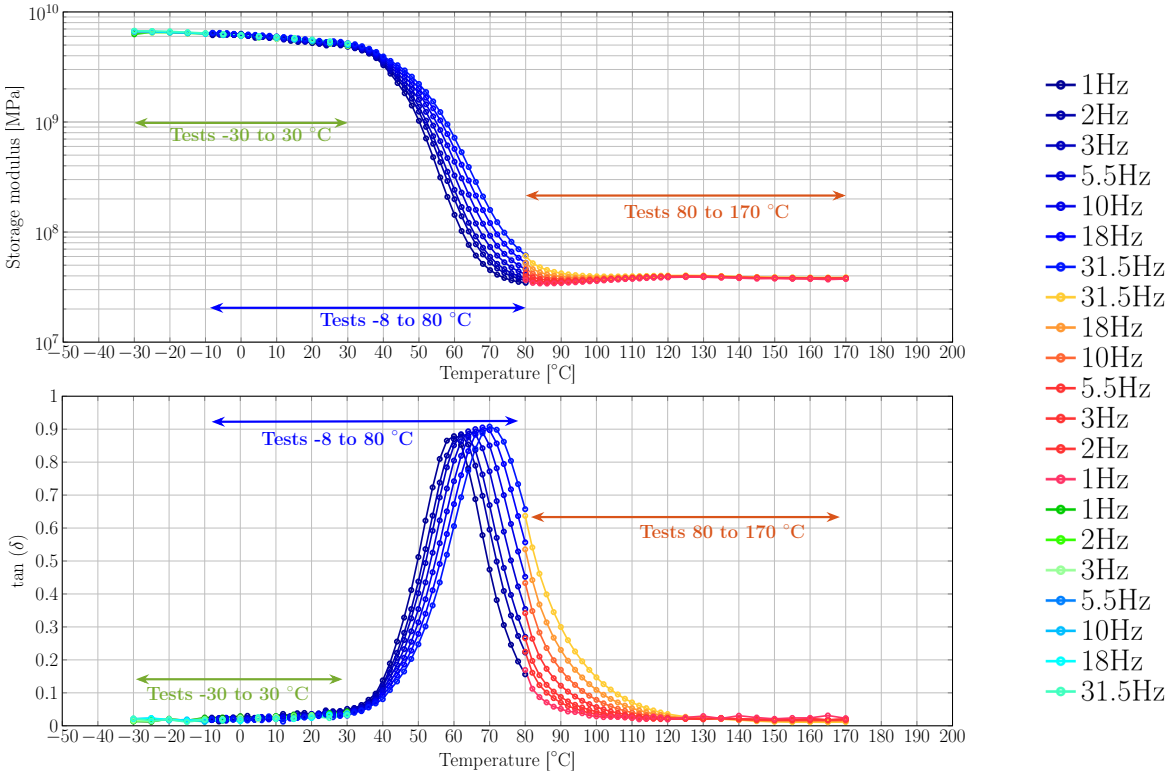

Fig. 6: Evolution of the storage modulus E' (a) and the loss factor η (b) according to the temperature for several frequencies for the resin A

Only the case of resin A is detailed in this section, the characteristics of the other resins are provided in Appendix 6. Through application of the Arrhenius law (Fig. 7), it is verified that viscoelastic resins comply with the Time-Temperature Superposition (TTS) principle. The coefficient of determination R^2 linking the experimental results and the Arrhenius model is very close to 1, meaning that the global behavior is well recovered. The small observed discrepancies result in slight errors when constructing the master curve, and in the long-term behavior, but it may not drastically affect short-term predictions on the domain of study. The master curve for the results is thus determined by applying the TTS principle, with the Arrhenius law providing the necessary temperature dependence to correctly shift the data. A fractional Zener model [**?**] is selected to describe the evolution of the behavior of the coating resins. The complex modulus hence writes

$$E^*(\omega_{a_T}) = \frac{E_0 + E_\infty (j\omega_{a_T}\tau)^\alpha}{1 + (j\omega_{a_T}\tau)^\alpha}. \tag{5}$$

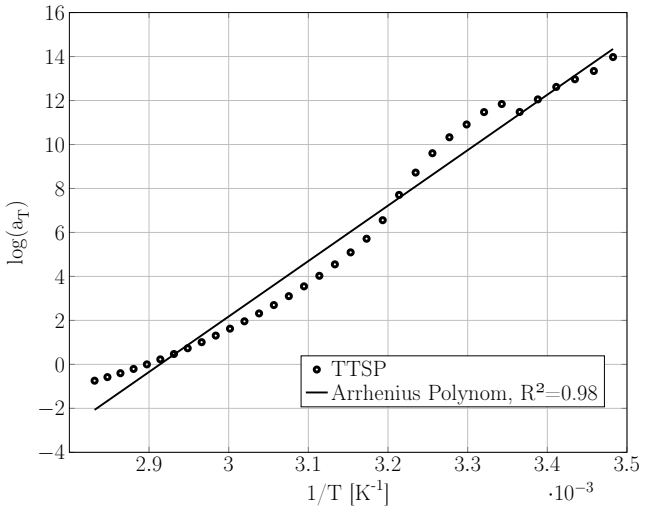

Fig. 7: Arrhenius law used to model the shift factor a_T according to T for resin A

The order of the fractional derivative α as well as the relaxation time of the material τ are determined by [**?**]

$$\alpha = \frac{2}{\pi}\arcsin\left(\eta_{max}(E_\infty - E_0)\frac{2\sqrt{E_\infty E_0} + (E_\infty + E_0)\sqrt{1+\eta_{max}^2}}{\eta_{max}^2(E_\infty + E_0)^2 + (E_\infty - E_0)^2}\right) \tag{6}$$

and

$$\tau = \frac{1}{2\pi a_T f_{\eta_{max}}}\left(\frac{E_0}{E_\infty}\right)^{\frac{1}{2\alpha}}. \tag{7}$$

Fig. 8 shows the fractional Zener model identified from the master curve of resin A obtained for a reference temperature T_0 of 72°C. The experimental and analytical master curves are close even if there are some differences. Experimentally, the high and low frequency moduli are not constant and the evolution of the loss factor is not perfectly symmetrical on both sides of η_{max}. More complex rheological models could be used for better correlation, such as the Generalized Maxwell Model [**?**], at the cost of higher number of parameters to identify. However, the parameters of the fractional Zener model have a strong physical meaning and are very good candidates to play with in optimization procedures whose results cane easily be handled by resin manufacturers.

Table 1 lists the parameters identified for the four resins from the master curves for a common reference temperature of 72°C. It is important to note that the glass-transition temperature is also frequency dependent.

	A	B	C	D
E_∞	4000 MPa	6000 MPa	5500 MPa	2500 MPa
E_0	20 MPa	220 MPa	55 MPa	25 MPa
T_g	$\sim 65\,^\circ$C	$\sim 110\,^\circ$C	$\sim 60\,^\circ$C	$\sim 20\,^\circ$C
$a_{72^\circ C} f_{\eta_{max}}$	93.65 Hz	3×10^{-8} Hz	140 Hz	2.5×10^4 Hz
η_{max}	0.95	0.8	0.85	0.85
E_a	2.1×10^5 J/mol	1.9×10^5 J/mol	1.9×10^5 J/mol	10^5 J/mol

Table 1: Fractional Zener model parameters for the resins

Finally, according to the fractional Zener model and the time-temperature superposition principle, the dynamic

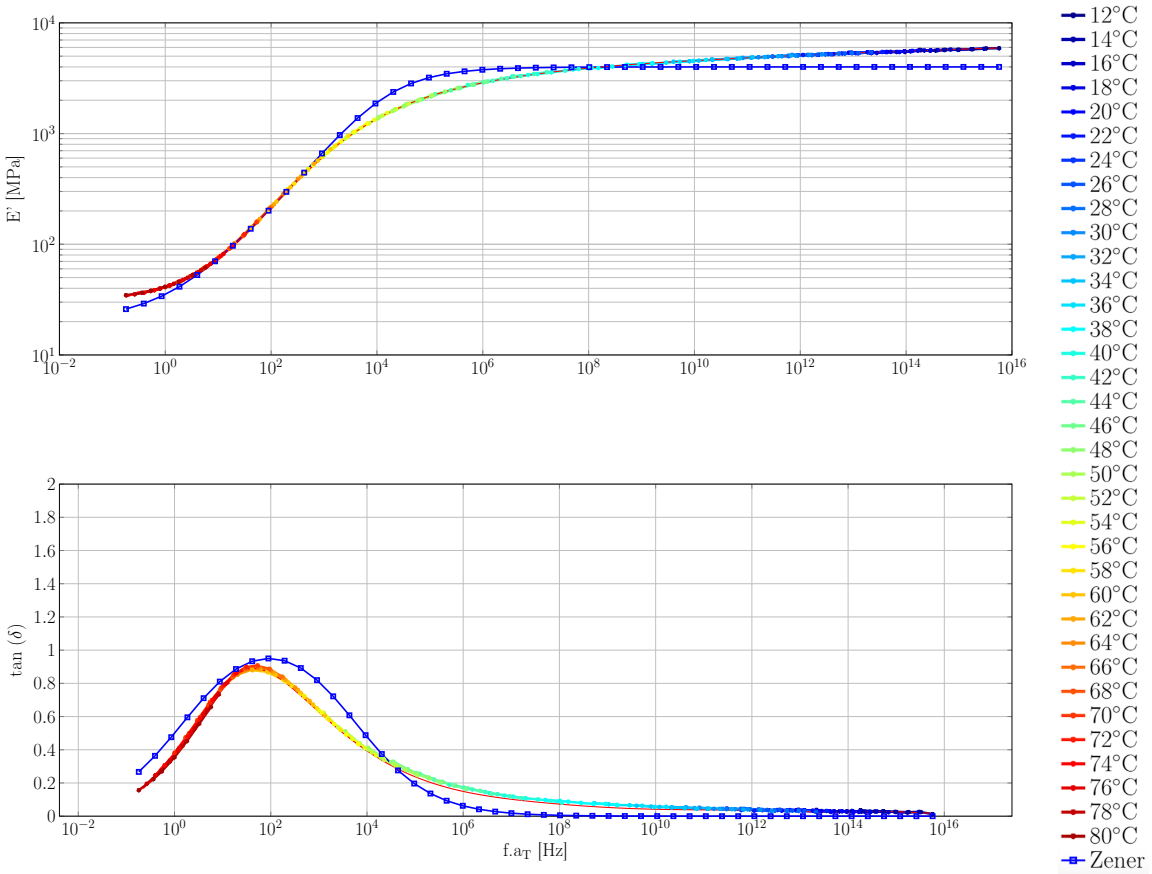

Fig. 8: Identified fractional Zener model for resin A

equation writes

$$-\omega^2 \mathbf{M}\hat{\mathbf{U}} + (1 + j\eta_e)\mathbf{K}_e\hat{\mathbf{U}} + \mathbf{K}_v \frac{E_0 + E_\infty (j\omega_{a_T}\tau)^\alpha}{1 + (j\omega_{a_T}\tau)^\alpha}\hat{\mathbf{U}} = \hat{\mathbf{F}}_e \tag{8}$$

with $\mathbf{K}_v$ the localization matrix associated to the potting resin. The validity of this equation is restricted to homogeneous potting, however it easily extends to non-homogeneous cases.

The equation to be solved includes a frequency-dependent stiffness matrix and the size of the operators is larger than 3.10^6 degrees of freedom which leads to very high calculation costs, about 36 min for a frequency step. The corrected ERP computation on a frequency band ranging from 400 to 8000 Hz and comprising at least 228 frequency steps, requires more than 5 days. Consequently, running a vibroacoustic optimization to find the optimal resin parameters is practically unrealistic. In this context, a model reduction strategy has been developed to significantly reduce the computation time and allow the optimization procedure.

3.2. Model reduction based on multi-model basis and vibroacoustic optimization

Due to the high frequency-dependency of the material behavior, no single model can typically represent the full complexity across the entire range of interest. Conventional reduction methods based on normal modes can be applied changing the calculation frequency but such an approach is clearly too costly in terms of computing time to allow the development of an optimization approach. The model reduction is a high challenge to solve an electric motor optimization problem involving advanced viscoelastic resin models. The methodology proposed here is the multi-model approach [**?**]. This approach has proved effective in reducing models involving

components with frequency- [? ? ?] or speed-dependent behavior [?], or highly damped components [?], and is thus a relevant approach for the case of electric motors in the presence of complex viscoelastic material modeling. The principle consists in building a projection basis taking into account the softening and stiffening of the resin as a function of the frequency. This basis is built by combining modal bases extracted for stiffness obtained at different frequencies. In the studied case and thanks to the time-temperature superposition principle, two modal bases are sufficient to represent the dynamics over the frequency and temperature ranges of interest: a basis representative of the low frequency (or high temperature) behavior $\mathbf{\Phi}_{LF}$ and a high frequency (or low temperature) basis $\mathbf{\Phi}_{HF}$. The number of bases selected should be adapted according to the case studied. To create $\mathbf{\Phi}_{LF}$ the p first modes are extracted by choosing ω equal to the minimum frequency ω_{Hf} of the studied interval and solving,

$$\left(-\omega_i^2\mathbf{M} + \mathbf{K}_e + \Re(\mathbf{K}_v \frac{E_0 + E_\infty (j\omega_{BF}\tau)^\alpha}{1 + (j\omega_{BF}\tau)^\alpha})\right)\phi_i = 0. \tag{9}$$

The high frequency basis $\mathbf{\Phi}_{HF}$ is obtained solving the same equation used to extract $\mathbf{\Phi}_{LF}$ but for $\omega = \omega_{HF}$ the maximum frequency of the studied interval.

Finally, the low frequency basis $\mathbf{\Phi}_{LF}$ is enriched by the high frequency basis $\mathbf{\Phi}_{HF}$ using a Gram-Schmidt orthonormalization with respect to mass matrix to ensure the good conditioning of the problem. This multi-model basis $\mathbf{\Phi}$ is then used to project the operators of the full FE model and the reduced system is therefore written,

$$-\omega^2\mathbf{m}\hat{\mathbf{q}} + (1 + j\eta_e)\mathbf{k}_e\hat{\mathbf{q}} + \mathbf{k}_v \frac{E_0 + E_\infty (j\omega_{a_T}\tau)^\alpha}{1 + (j\omega_{a_T}\tau)^\alpha}\hat{\mathbf{q}} = \hat{\mathbf{f}}_e, \tag{10}$$

where $\mathbf{m} = \phi^T\mathbf{M}\phi$, $\mathbf{k_e} = \phi^T\mathbf{K_e}\phi$, and $\mathbf{k_v} = \phi^T\mathbf{K_v}\phi$ are respectively the modal mass matrix, the modal stiffness matrix for the non-resin part and for the potting, and $\hat{\mathbf{f}}_e = \boldsymbol{\phi}^T\hat{\mathbf{F}}_e$ is the projected load vector. $\hat{\mathbf{q}}$ is the generalized coordinate vector such that $\hat{\mathbf{U}} = \boldsymbol{\phi}\hat{\mathbf{q}}$.

From a practical standpoint, DMAPs were developed to create and use this type of enriched basis to use the NASTRAN solver. Fig. 9 shows the comparison between a direct calculation of the ERP (with a radiation factor equal to 1) from the complete FE model (SOL 108 in NASTRAN) and after projection on the multi-model basis (SOL 111 in NASTRAN). The proposed approach captures well the behavior specific to viscoelastic systems and the computation times are drastically reduced: 6 days 4 hours and 14 minutes for 242 frequency steps in SOL108 against 54 min for 2501 frequency steps in SOL 111. Fig. 10 shows the flowchart covered so far and how the corrected ERP is calculated.

By following this updated workflow, it is now possible to quickly calculate the Equivalent Radiated Power of the electric motor by taking into account the viscoelastic behavior of the potting resin and the radiation factor σ:

$$ERP_{dB}^{\sigma} = 10\log\left(\frac{\sigma(\omega)ERP(\omega)}{1 \times 10^{-12}}\right). \tag{11}$$

Fig. 11 presents the ERP_{dB}^{σ} calculated when the engine is coated with resin A, for two different temperatures (40°C and 120°C). At 40°C, the resin is in its glassy state and the mode (2.0) is outside the frequency band of interest. The maximum ERP_{dB}^{σ} is around 80 dB. However, when the temperature increases and exceeds the glass transition temperature of the resin (65°C for resin A), the elastic modulus decreases, which leads to an overall softening of electric motor dynamic behavior. The radiating mode is then found in the frequency band

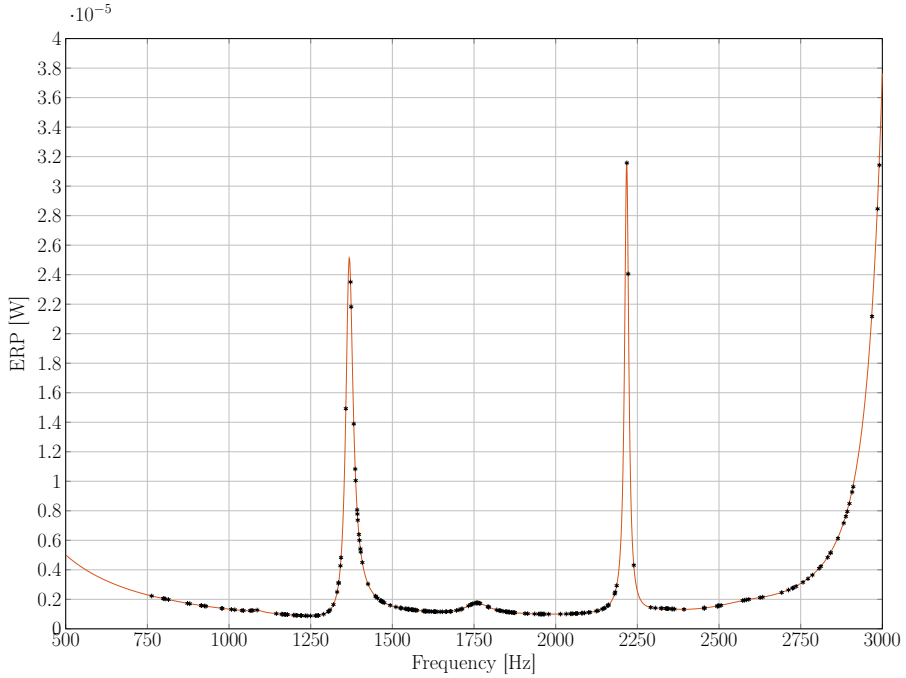

Fig. 9: Validation of the multi-model approach: – NASTRAN SOL 111 with multi-model basis, $f_{LF} = 5\,\text{Hz}$, $f_{HF} = 3000\,\text{Hz}$, 2501 steps, 54 min ; *** NASTRAN SOL 108, Reference, 242 steps, 6 days 4h 14 min.

of interest and the maximum ERP^{σ}_{dB} is 92 dB.

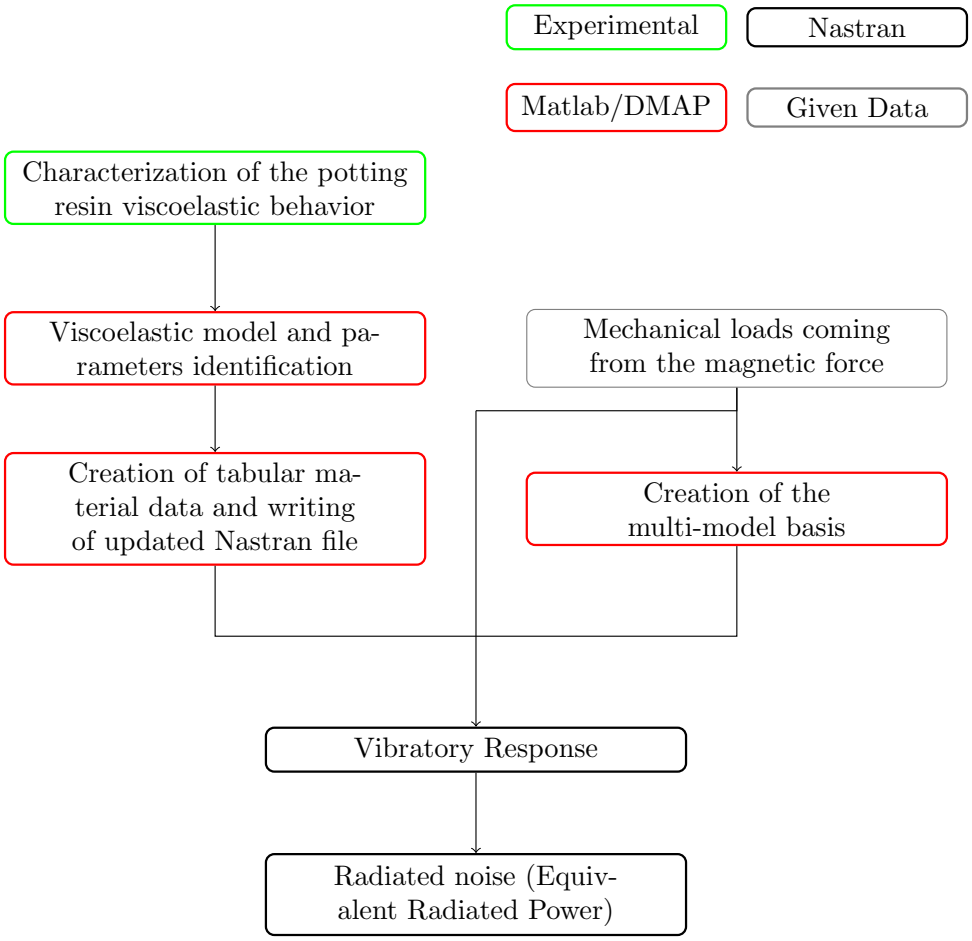

Fig. 10: Updated workflow

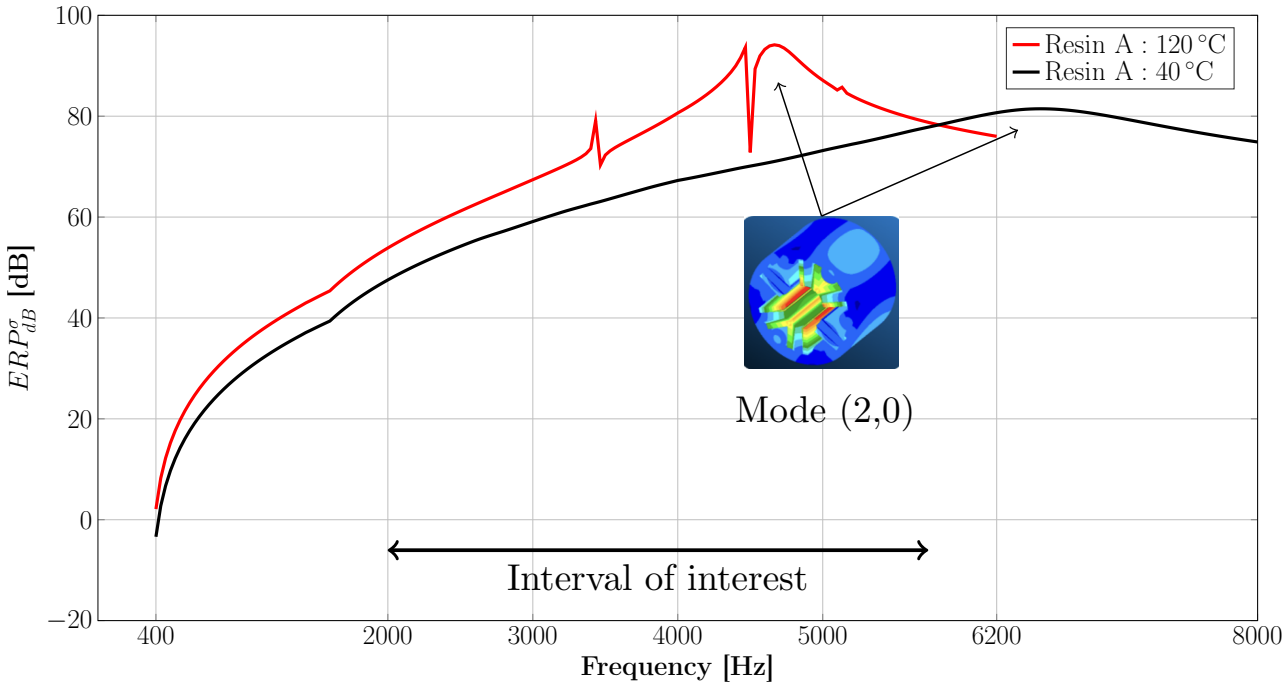

Fig. 11: ERP^{σ}_{dB} calculated at 40 and 120°C for the motor coated with resin A

3.3. Vibroacoustic optimization procedure

The objective is to minimize the radiated noise by the electric motor over a frequency band from 2000 to 6000 Hz and a temperature interval ranging from 40 to 140 °C by optimizing the viscoelastic properties of the potting resin. Fig. 12 shows the workflow used during optimization and several DMAP routines have been developed to link MATLAB and the NASTRAN solver. The optimization process aims at finding the parameters of an optimal fractional Zener model.

A preliminary parameter analysis is required to reduce the number of parameters and fasten the optimization process. First, the maximum loss factor η_{max} is fixed to 0.85 because as it does not vary much from one tested resin to another. However, considering the loss factor as an optimization parameter would be of interest in some situations, providing the available resins can be elaborated with the corresponding properties. The activation energy E_a is arbitrarily fixed at 2×10^5 J/mol. As a consequence, only the parameters E_0, E_∞, and $f_{\eta_{max}}$ are selected for the optimization. To be confident in the ability of resin manufacturers to formulate the required chemistry, the evolution of these parameters is bounded according to the results of the experimental characterization (Table 1). However, the glass transition temperature bounds are extended as it is possible to play with this parameter during the resin elaboration process. As a first step, the objective function aims at minimizing the maximum value of ERP^{σ}_{dB} on the frequency ($\Delta\omega$) range of interest, for a single temperature T. In this case, the optimization problem is described in Fig. 13.

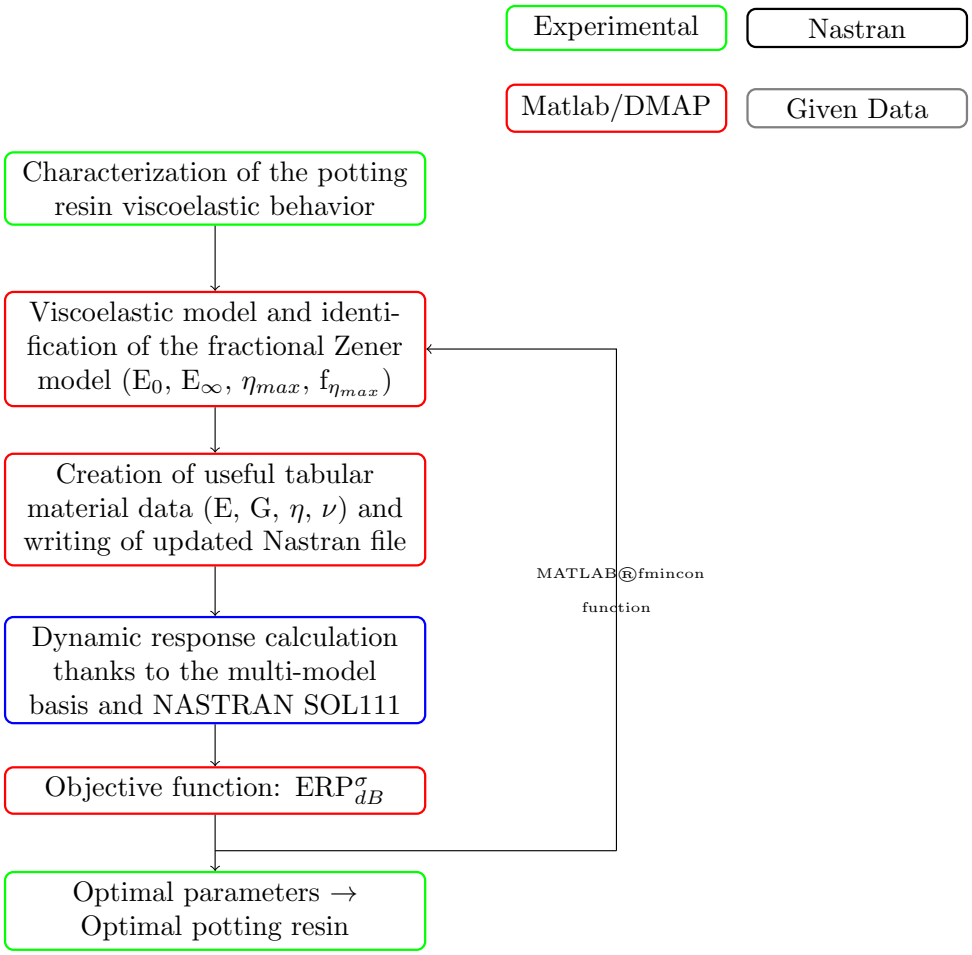

Fig. 12: Optimization workflow

Given	T, $\Delta\omega$
Find	$E_0, E_\infty, \eta_{max}, f_{\eta_{max}}$
Minimizing	$f_{cost} = \|\|ERP^{\sigma}_{dB}(\omega, E_0, E_\infty, \eta_{max}, f_{\eta_{max}})\|\|_\infty$
Subject to	$-\omega^2\mathbf{m}\hat{\mathbf{q}} + (1+j\eta_e)\mathbf{k}_e\hat{\mathbf{q}} + \mathbf{k}_v\frac{E_0+E_\infty(j\omega a_T\tau)^\alpha}{1+(j\omega a_T\tau)^\alpha}\hat{\mathbf{q}} = \hat{\mathbf{f}}_e$
	$25\,\text{MPa} \leqslant E_0 \leqslant 220\,\text{MPa}$
	$2500\,\text{MPa} \leqslant E_\infty \leqslant 6000\,\text{MPa}$
	$\eta_{max} = 0.85$
	$1\times10^{-17}\text{a.Hz} \leqslant f_{\eta_{max}} \leqslant 3\times10^{4}\text{a.Hz}$

Figure 13: Optimization procedure for a single temperature

In case the optimization is related to a temperature range ΔT instead of a single one, the multi-objective problem is solved by scalarization which consists in which consists in transforming the problem into a single-objective problem, where in this case the same weight is applied to all objectives. The objective function to be minimized can thus be chosen as the average of the maximum $ERP_{[}dB]^{\sigma}$ computed for N_T values of temperature $T_i \in \Delta T$,

$$f_{cost} = \frac{1}{N_T}\sum_{i=1}^{N_T}||ERP^{\sigma}_{dB}(\omega, T_i, E_0, E_\infty, \eta_{max}, f_{\eta_{max}})||_\infty. \tag{12}$$

The optimization process is run using parameters of resin B as initial parameters because the noise level obtained with this resin is low prior to any optimization process, and thus this resin is an interesting reference case. Fig. 14 shows the convergence curve obtained for the vibroacoustic optimization at a temperature of 140 °C. The optimization is performed in 4 h 26 min thanks to the multi-model approach.

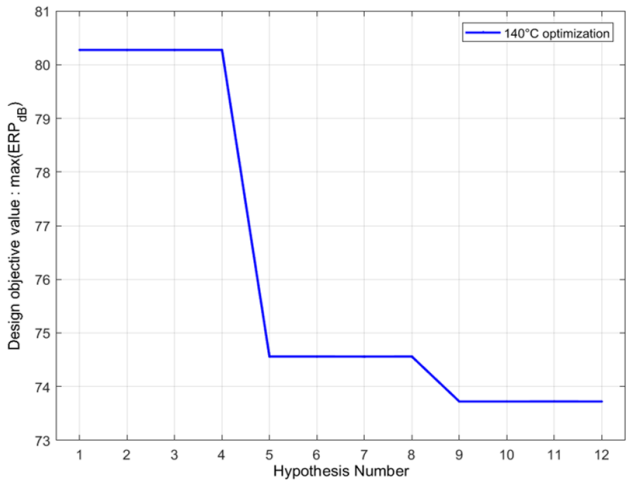

Fig. 14: Convergence curve for solving the vibroacoustic optimization problem at 140°C

4. Results and discussions

When the optimization is carried out for a temperature of 40 °C , the values obtained for the parameters are $E_0 = 125\,\text{MPa}$, $E_\infty = 5985\,\text{MPa}$, $a_{72°C}f_{\eta_{max}} = 9.98\times10^{-8}\,\text{Hz}$, and for an optimization for a temperature of 140 °C the values are $E_0 = 216.5\,\text{MPa}$, $E_\infty = 5985\,\text{MPa}$, $a_{72°C}f_{\eta_{max}} = 1.1\times10^{-15}\,\text{Hz}$. Fig. 15 presents the evolution of the ERP^{σ}_{dB} on the frequency band of interest for the two temperature cases (40 °C - case (a)

and 140 °C - case (b)). For the two temperatures, the solution obtained with the initial parameters for the fractional Zener model and resin B is compared to results given by the optimization, considering three Zener parameters (E_0, E_∞, $f_{\eta_{max}}$), or only one ($f_{\eta_{max}}$) as optimization variables. Since the frequency band over which the radiated noise must be reduced is quite narrow (2000 Hz to 6000 Hz), the optimization process leads to remove mode $(2, 0)$ from this frequency range. This is a feasible solution as the optimal parameters remain in the bounds corresponding to the tested resins.

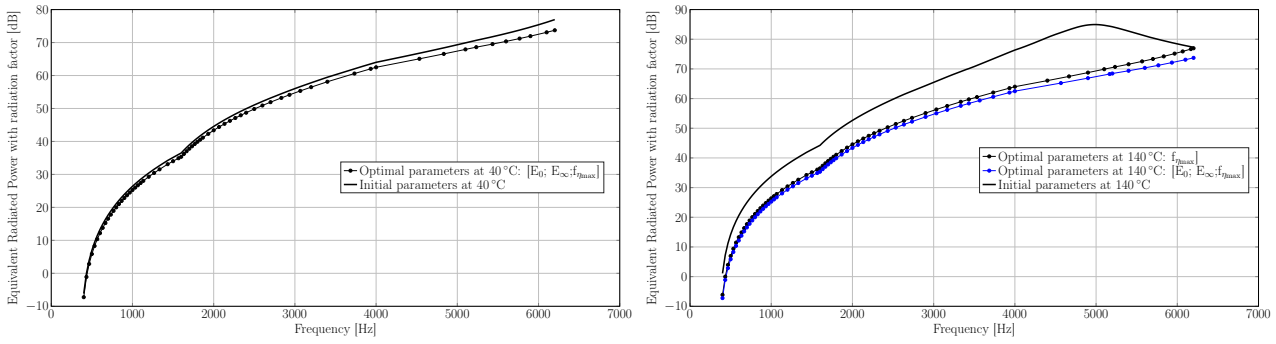

(a) (b)

Fig. 15: ERP^{σ}_{dB} at 40°C (a) and 140°C (b) for the fractional Zener initial parameters and for the optimal ones on the frequency band of interest. Different optimization studies are done considering three Zener parameters (E_0, E_∞, $f_{\eta_{max}}$), or only one ($f_{\eta_{max}}$).

In the case where the temperature of the resin is 40 °C (Fig. 15(a)), with the initial parameters, the glass transition temperature of the resin is around 110 °C, and therefore already above 40 °C. Thus, to minimize ERP^{σ}_{dB}, the optimization results in increasing the high frequency modulus value E_∞ up to 5985 MPa, with an upper bound fixed to 6000 MPa. This modification tends to stiffen the dynamic behavior of the electric motor and therefore to push the radiating mode towards high frequencies.

At 140 °C (Fig. 15(b)), the optimization converges after increasing the two asymptotic moduli E_0 and E_∞ respectively up to 216.5 MPa (upper limit 220 MPa) and 5985 MPa (upper limit 6000 MPa), and reduces the reduced frequency at which the maximum damping is observed $a_{72°C} f_{\eta_{max}} = 1.12 \times 10^{-15}$ Hz (lower limit 1×10^{-17} Hz). It should be noted that the ERP^{σ}_{dB} evolution on the frequency band of interest, after optimization of the viscoelastic properties of the potting resin is similar at 40 and 140 °C.

Within the framework of the study presented in this paper and for the temperature and frequency bands of interest, respectively $[40; 140]$°C and $[2000; 6000]$Hz, it does not seem necessary to solve an optimization for a set of temperatures since the optimal solution at 140°C which is close to optimal for lower temperatures as shown in Fig. 16.

In terms of design of the potting resins, the results of the optimization for the considered configuration show that it is necessary to focus on a resin that is as rigid as possible (asymptotic moduli) and having a high glass transition temperature. Moreover, it should be noted that if the mode $(2, 0)$ had been out of the frequency band of interest for the studied temperature range, or if several radiating modes had been present, it would have been interesting to carry out an optimization on a set of temperatures using the objective function (Eq. 12) to determine the best trade-off. Finally, in the study, the bounds of the design variables correspond to the range of properties measured on the different of potting resins presented in Section 3. By relaxing the constraints, it would undoubtedly be possible to achieve configurations that further reduce the Equivalent Radiated Power.

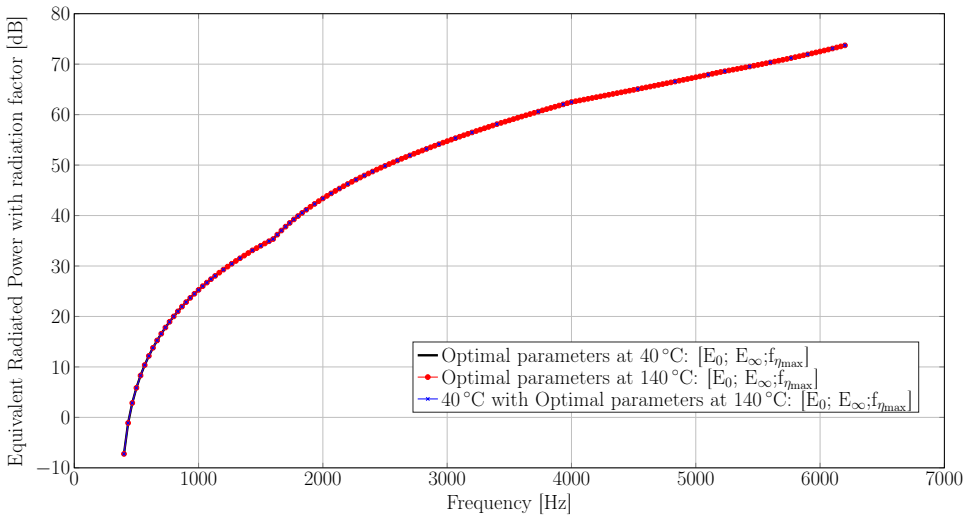

Fig. 16: ERP^{σ}_{dB} evolution according to the frequency at 40°C (blue dot) and 140°C (red cross) with the optimal viscoelastic properties obtained at 140°C

5. Experimental validation

The aim of this section consists in validating the previous results by implementing the potting using an optimal viscoelastic resin. As the authors do not possess the required skills to elaborate on-demand polymers, it was decided to find a resin on-the-shelf with properties as close as those computed in the previous section, ie. as rigid as possible (as the optimal values of E_0 and E_∞ were close to the upper bounds) and with a high glass transition temperature. The selected resin is referred as E. Its properties are given in table 2 : they have been measured following the same procedures as for resins A to D.

	E
E_∞	4000 MPa
E_0	100 MPa
T_g	$\sim 20\,^{\circ}$C
$a_{72^{\circ}C} f_{\eta_{max}}$	1×10^{-17} Hz
η_{max}	0.8
E_a	10^5 J/mol

Table 2: Fractional Zener model parameters for resin E

Fig. 17 presents a picture of the resin-coated electric motor.

Acoustic measurements were made in an anechoic environment, as shown in Fig. 18. The electric motor is suspended thanks to cables to be in free boundary conditions, two accelerometers are glued on the stator for vibratory measurements, two microphones are positioned at 90° at 1 m to measure the acoustic radiation. A thermocouple is used to control the temperature level.

Fig. 19 shows the acoustic pressure level measured at 1 m from the electric motor during an increase in rotational speed from 0 to 125 000 rpm for different configurations: motor without resin (▪·▪·), motor with the optimal resin for a temperature of 70 °C (▬) and a temperature of 130 °C (▬). The rise in temperature is a consequence of the operation of the engine. The optimal resin provides a significant acoustic gain since the noise level around the critical speed at 61 000 rpm is reduced by 38 dB. Thus, the resin here succeeds in achieving its intended purpose which was to minimize the infinite norm of the radiated noise, i.e. the maximum level of noise. The addition of stiffness with the resin pushes the ovalization mode, which is mainly responsible for the radiation, out

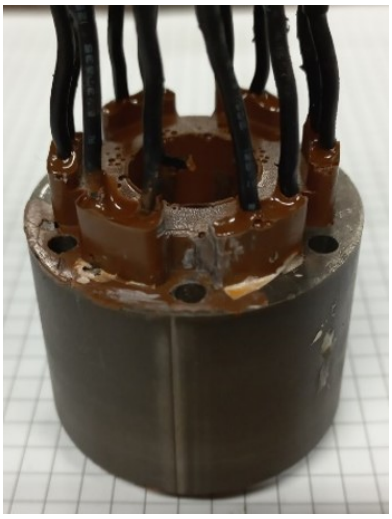

Fig. 17: Stator with the potted resin.

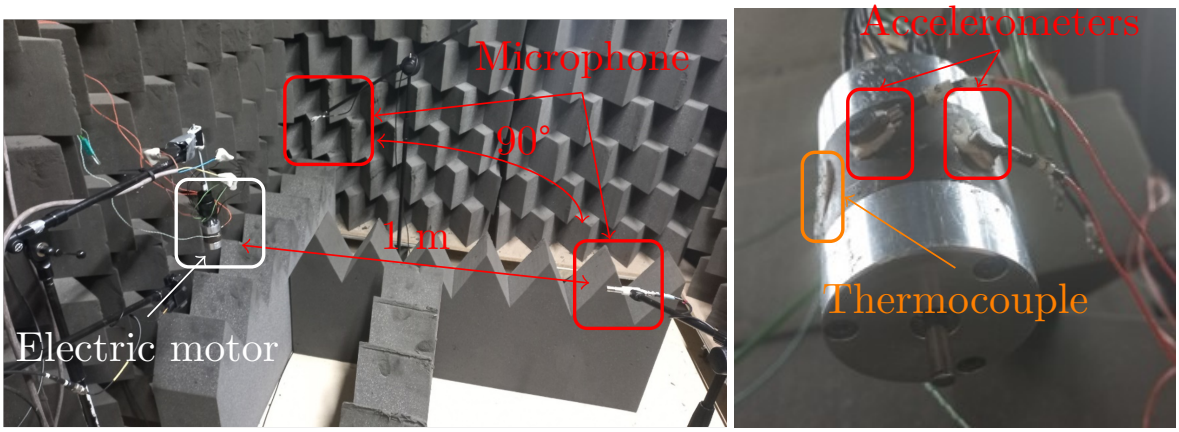

(a) (b)

Fig. 18: Experimental setup for acoustic and vibratory measurements on the electric motor: (a) Global overview, (b) Zoom on the motor

of the frequency band excited during operation. The acoustic performance is preserved during the temperature rise since the glass transition temperature of the selected resin is higher than the operational temperature. The stiffness properties are thus maintained.

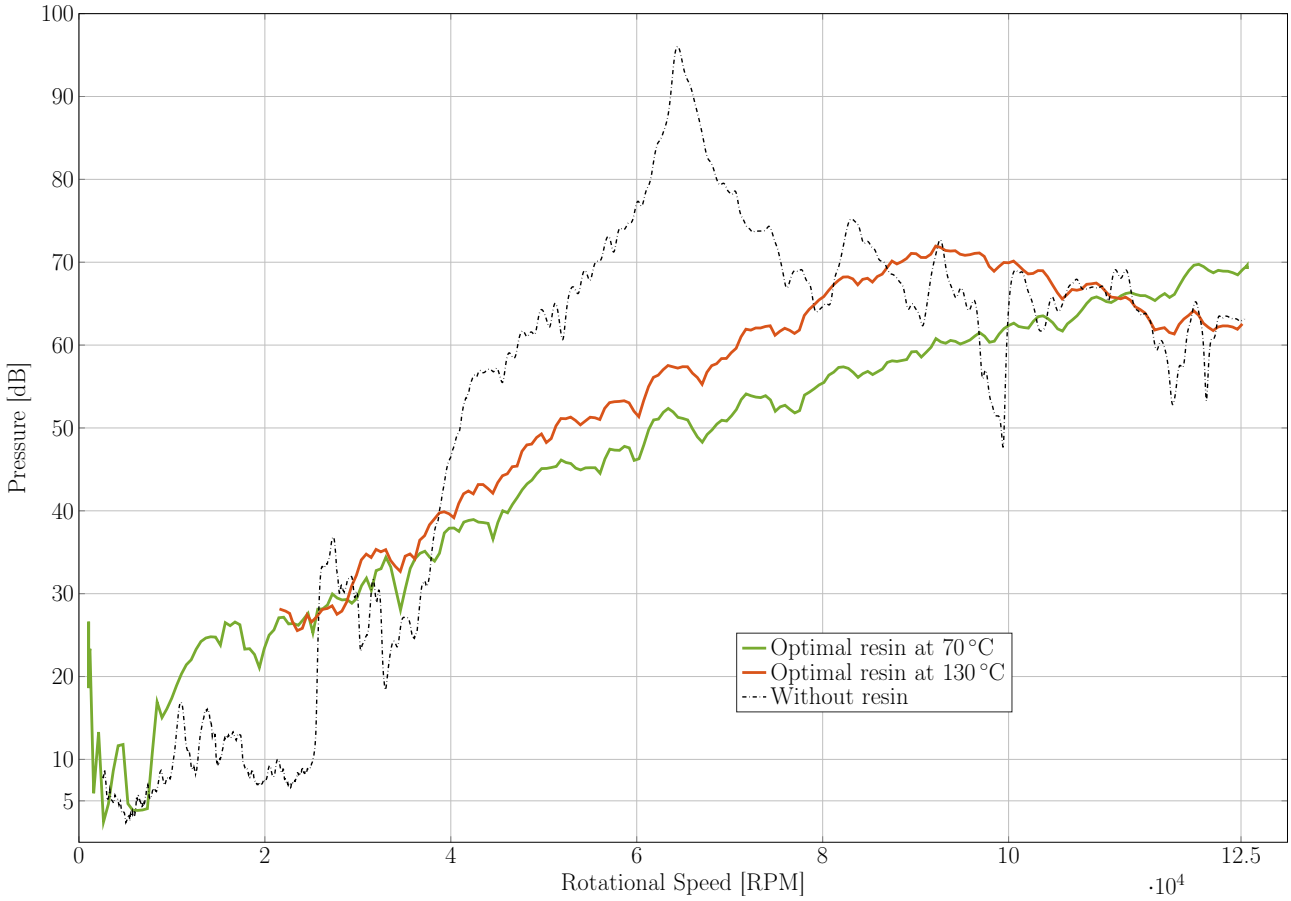

Fig. 19: Comparison of the acoustic pressure level radiated by the electric motor for different configurations: without resin, with the optimal resin at a temperature of 70°C and with the optimal resin at a temperature of 130°C.

6. Conclusions

This research work aims at taking advantage of the mechanical behavior of viscoelastic resins used in the coating of electric motors for the reduction of their acoustic radiation. These resins exhibit a frequency- and temperature-dependent behavior, which can thus be optimized to reduce the vibration and acoustic levels.

For that purpose, an approach has been developed to estimate the noise radiated by an electric motor potted with viscoelastic resins, and to identify optimal properties to minimize the radiated noise. First the dynamic mechanical properties of a set resin have been identified as a function of frequency and temperature using a Dynamic Mechanical Analysis, and a fractional Zener model has been used to describe the viscoelastic behavior. The dynamic behavior of the motor including the resins can thus be accurately estimated by introducing this model in the dynamic equation. Then, to drastically reduce calculation times and make optimization possible, a multi-model reduction method is implemented to capture the dynamic behavior evolution as a function of frequency and temperature. The approach has been implemented in an industrial case, demonstrating that it is possible to estimate with precision and at a low computational cost the dynamic behavior of a structure in the presence of a viscoelastic material. Finally, a method for optimizing the mechanical properties of resins to minimize radiated noise over given temperature and frequency ranges has been developed. Numerical simulations as well as experiments carried out on an engine equipped with a resin selected for its properties confirm that an adequate choice of resin makes it possible to considerably reduce the radiated noise.

The methodological developments of the research work in parametric identification of viscoelastic resin, dynamic

simulation with viscoelastic materials, and model reduction in the presence of frequency dependent parameters allow the design of an optimized resin for acoustics. It is important to emphasize that the approach developed takes precise account of the resin in terms of quantity introduced and positioning, and relies here on the functionalization of resin already used for protection or mechanical integrity purposes. The application potential is greater for machines that allow the addition of resins between teeth, such as variable reluctance machines, which are reputed to be particularly noisy and for which there are no noise control solutions at source. Thus, the proposed work paves the way to new considerations around potting resins in the field of electric motors.

Acknowledgements

The project e-silence was selected in the framework of the call for projects FUI-AAP23 of the Single Inter-Ministerial Fund (FUI). It is subsidized by the Public Investment Bank (BPI France) and the AURA region via the European Regional Development Fund (FEDER - this project is co-financed by the European Union). The research work has been supported by the EUR EIPHI Project (contract ANR-17-EURE-0002), Bourgogne-Franche-Comté Region, and Grand Besançon. The authors would like to thank the Von Roll company for providing the viscoelastic resins.

Appendices

The appendix presents the characterization and identification works carried out on resins B, C, D, E mentioned in Sec.3.

Characterization results for resin B

Fig. 20 presents the arrhenius law and the evolution of the Young modulus and loss factor for resin B. Fig. 21 presents the identifed frac- tional Zener model for resin B.

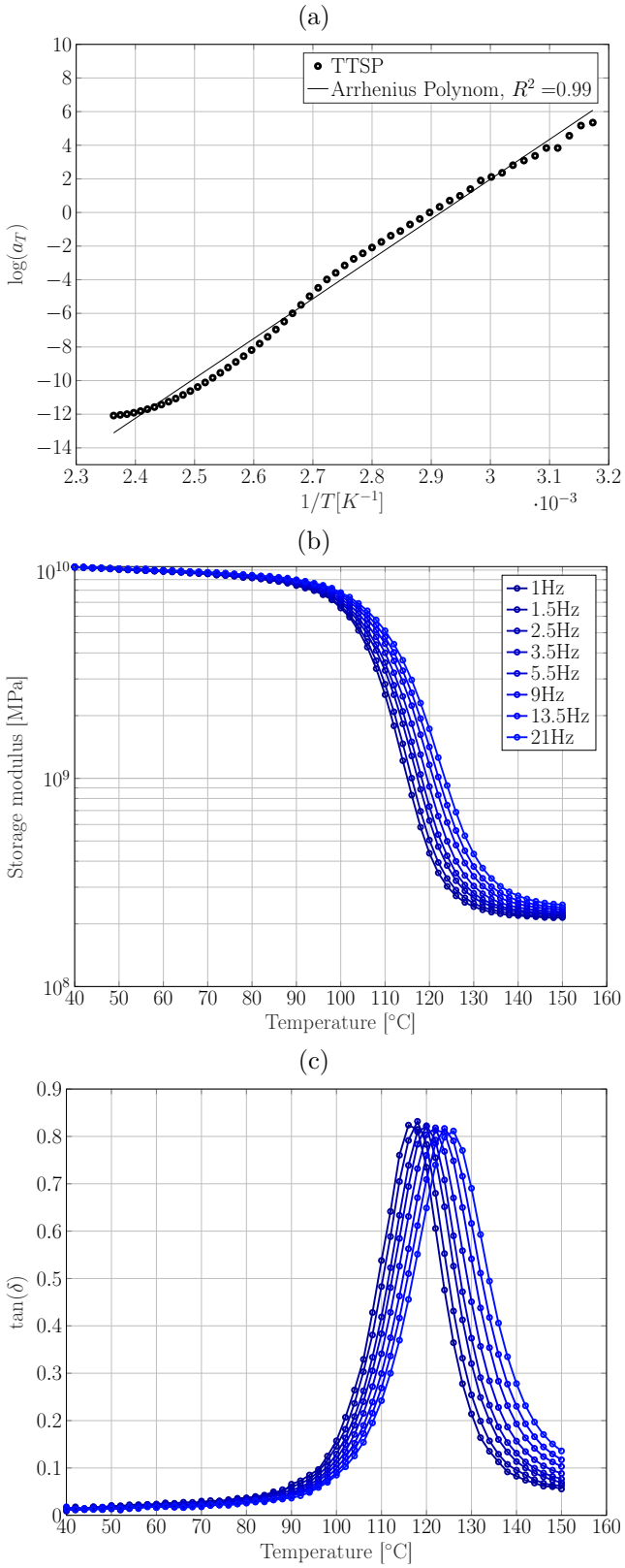

Fig. 20: Resin B : (a) Arrhenius law used to model the shift factor a_T according to T ; Evolution of the Young modulus (b) and of the loss factor η (c) according to the temperature for several frequencies.

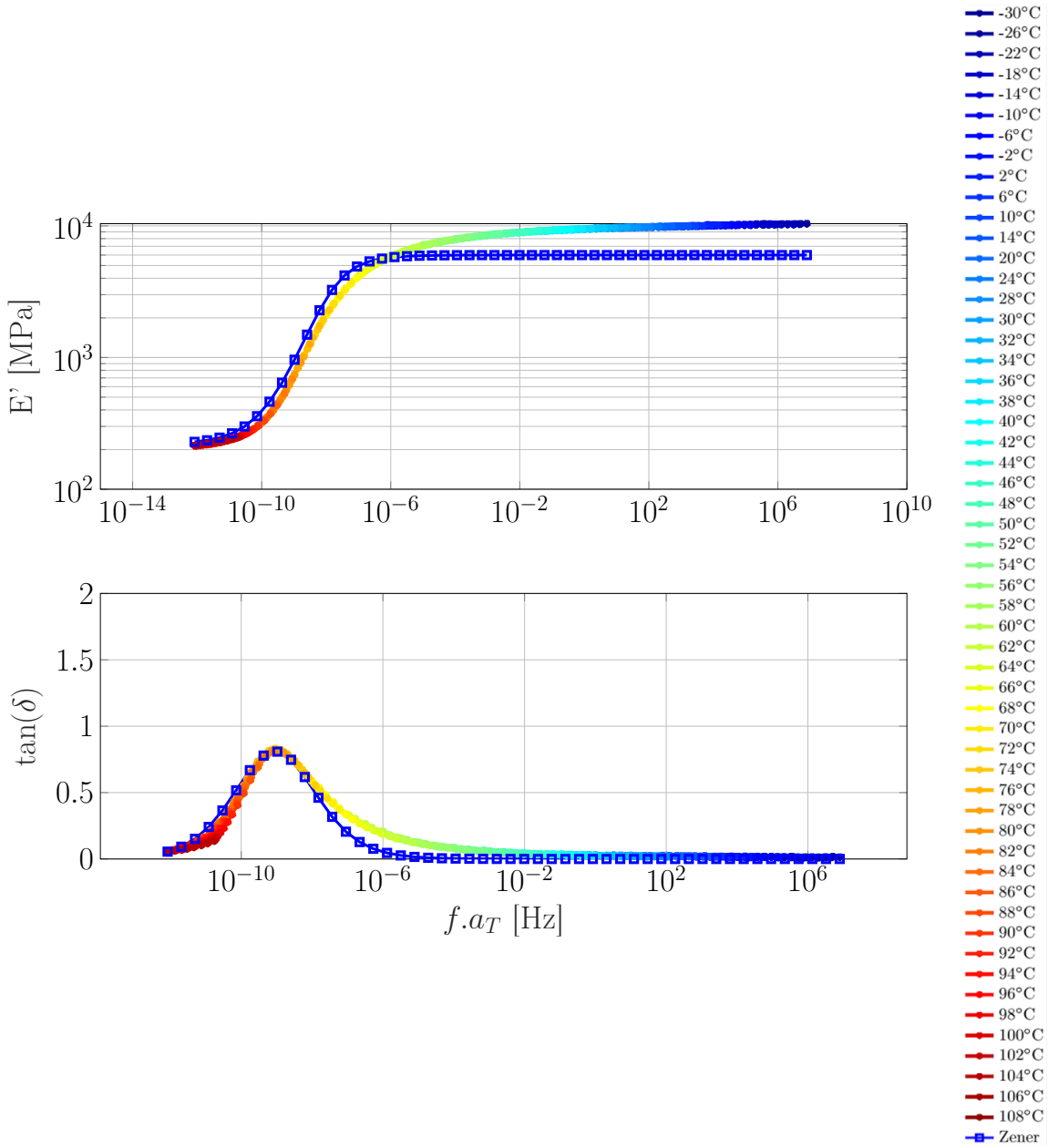

Fig. 21: Resin B : Identified fractional Zener model.

Characterization results for resin C

Fig. 22 presents the arrhenius law and the evolution of the Young modulus and loss factor for resin C. Fig. 23 presents the identifed frac- tional Zener model for resin C.

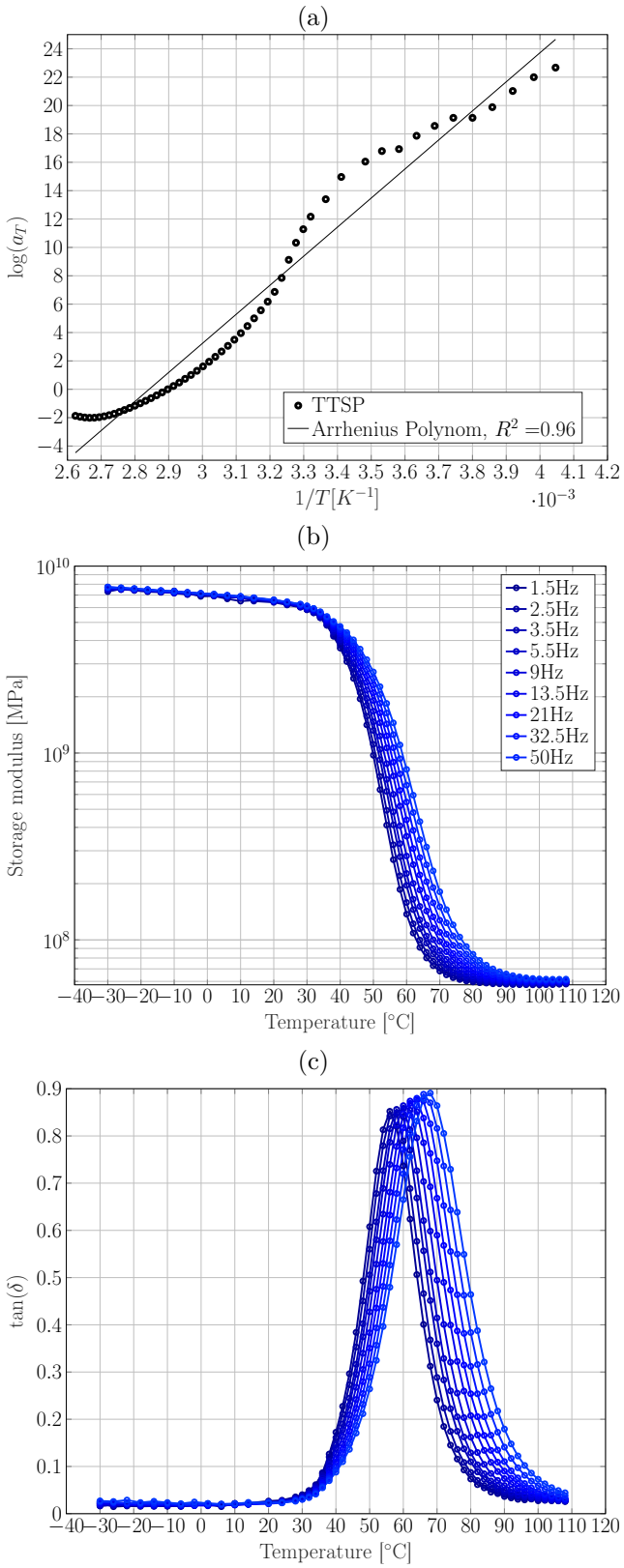

Fig. 22: Resin C : (a) Arrhenius law used to model the shift factor a_T according to T ; Evolution of the Young modulus (b) and of the loss factor η (c) according to the temperature for several frequencies.

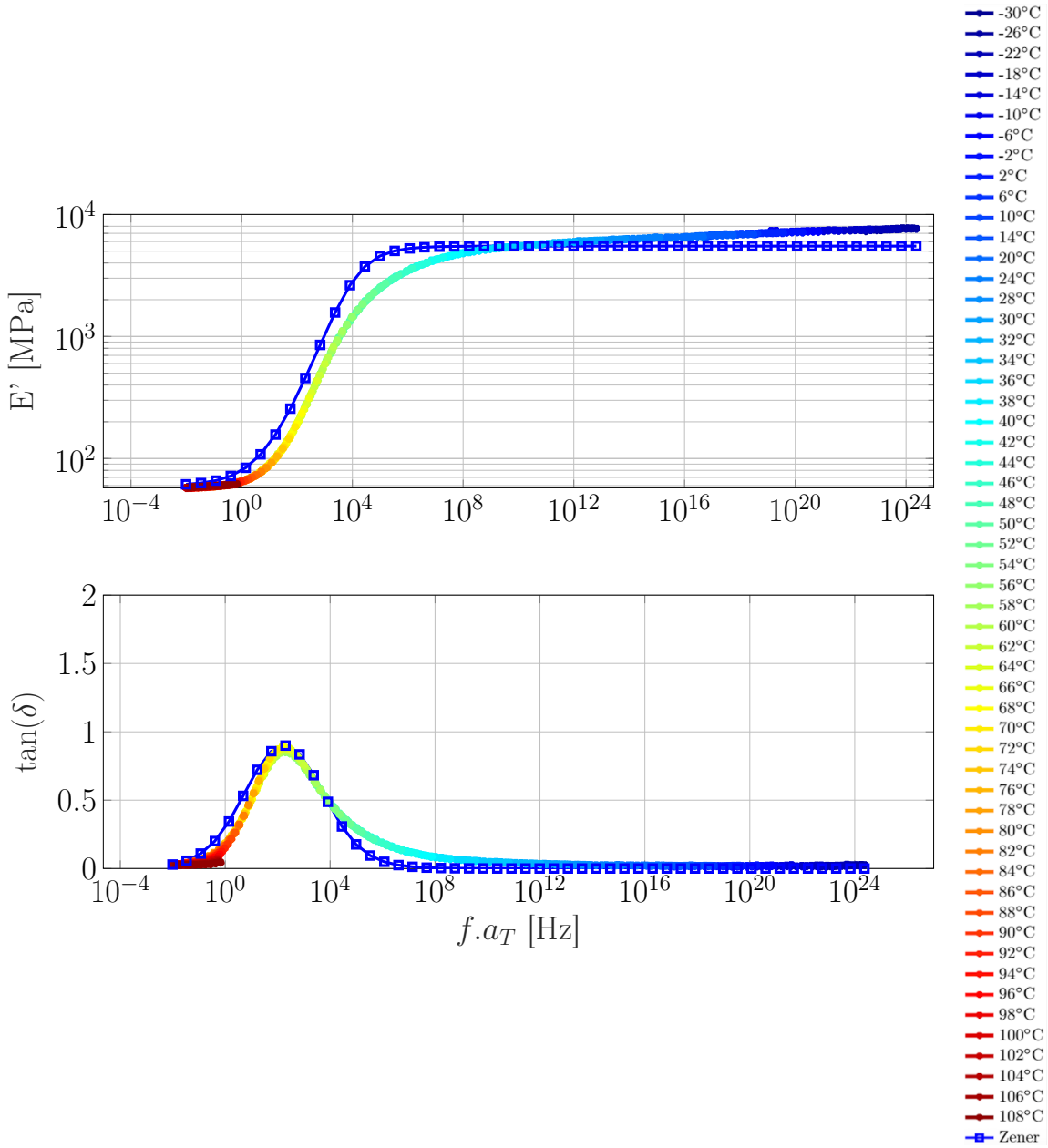

Fig. 23: Resin C : Identified fractional Zener model.

Characterization results for resin D

Fig. 24 presents the arrhenius law and the evolution of the Young modulus and loss factor for resin D. Fig. 25 presents the identifed frac- tional Zener model for resin D.

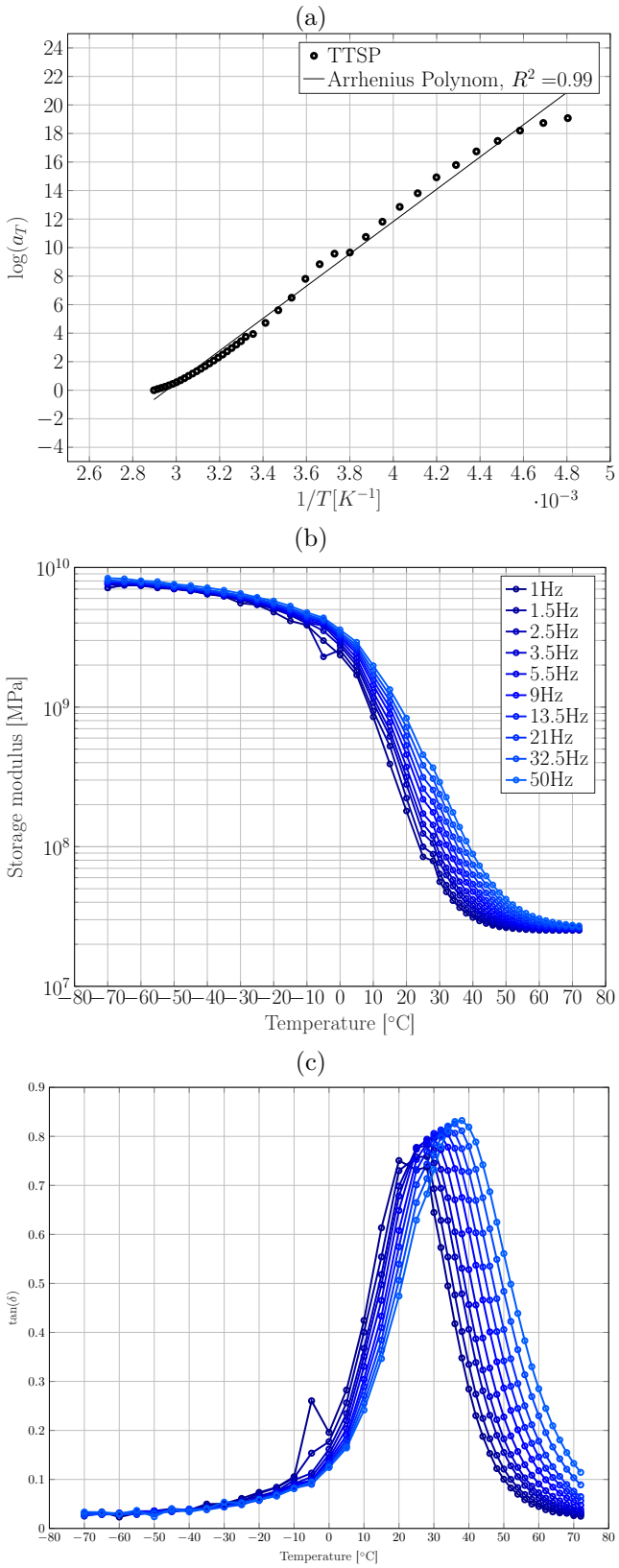

Fig. 24: Resin D : (a) Arrhenius law used to model the shift factor a_T according to T ; Evolution of the Young modulus (b) and of the loss factor η (c) according to the temperature for several frequencies.

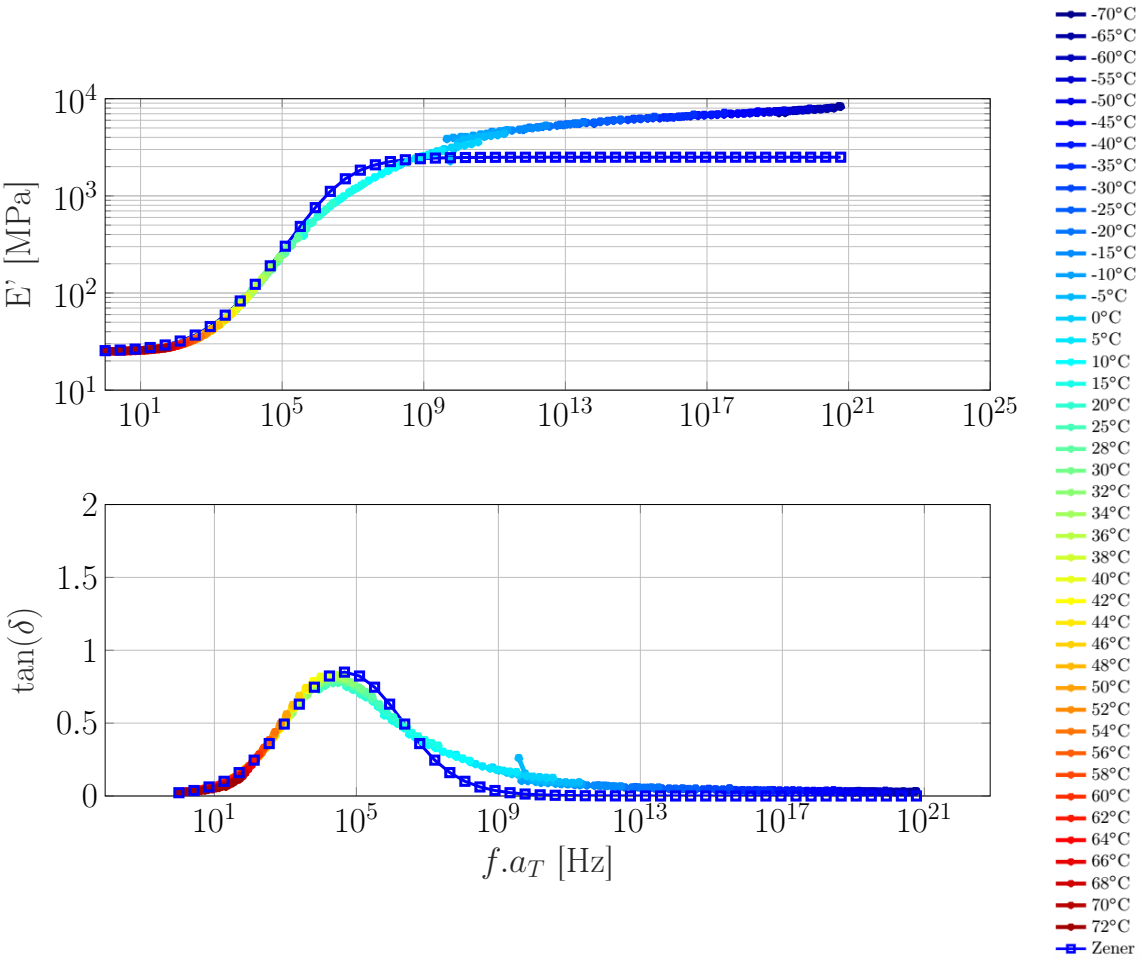

Fig. 25: Resin D : Identified fractional Zener model.

Characterization results for resin E

Fig. 26 presents the arrhenius law and the evolution of the Young modulus and loss factor for resin E. Fig. 27 presents the identifed frac- tional Zener model for resin E.

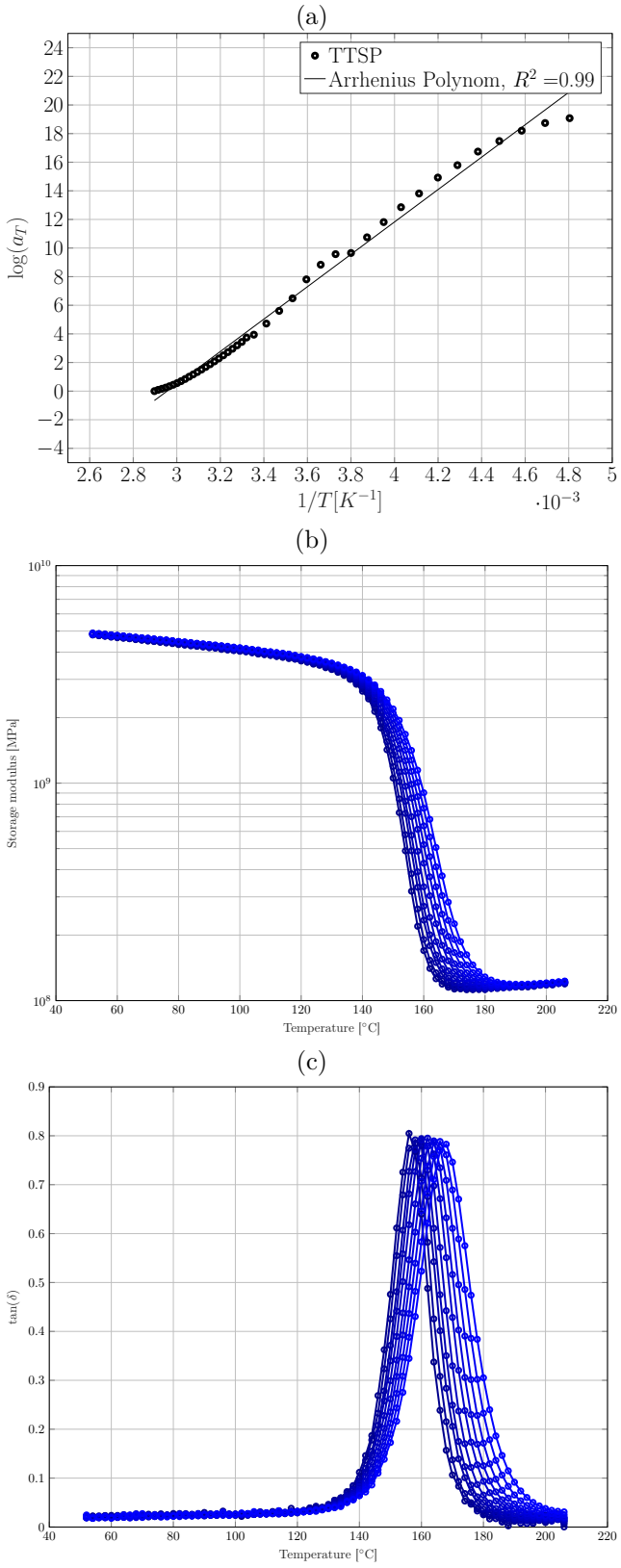

Fig. 26: Resin E : (a) Arrhenius law used to model the shift factor a_T according to T ; Evolution of the Young modulus (b) and of the loss factor η (c) according to the temperature for several frequencies.

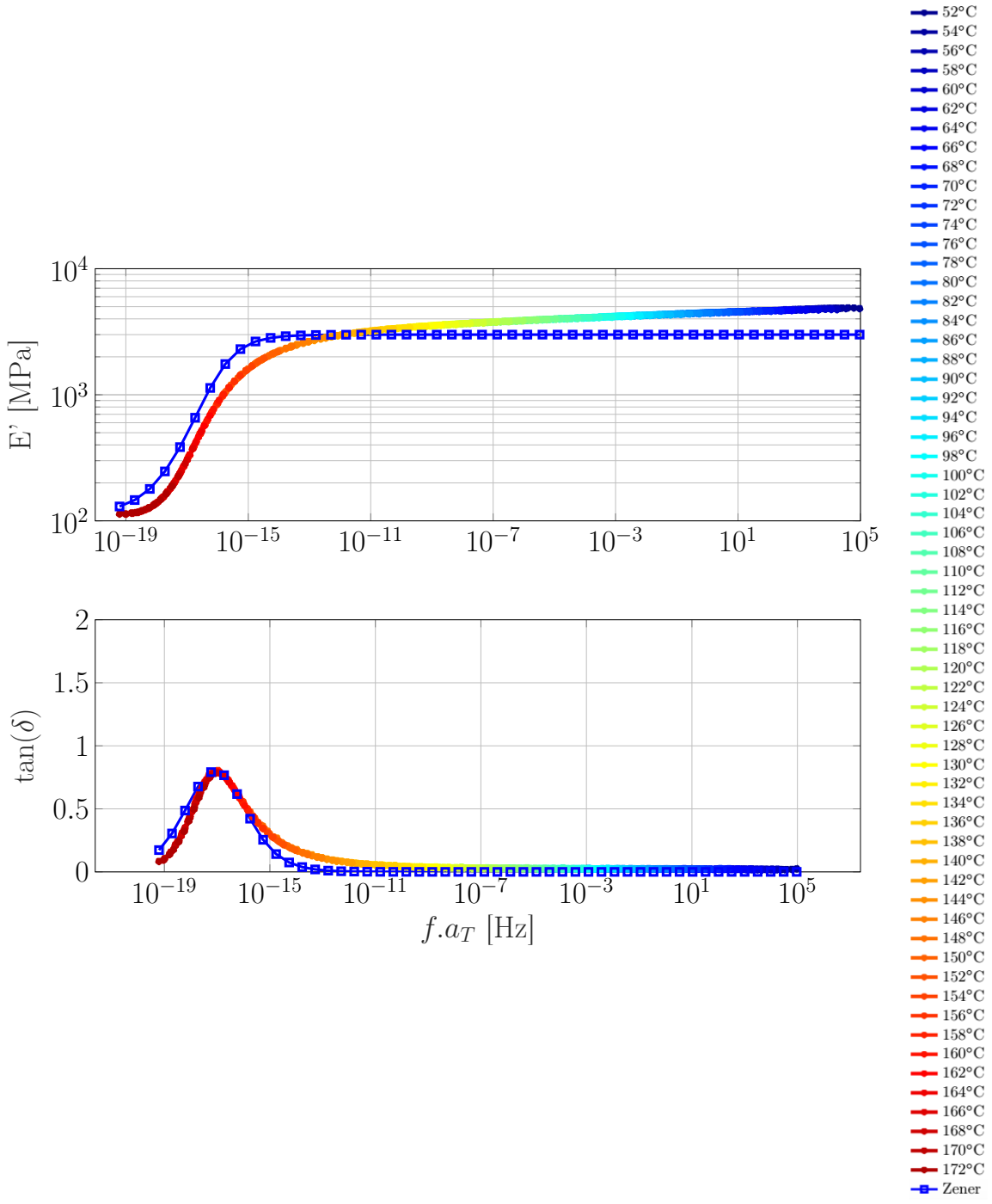

Fig. 27: Resin E : Identified fractional Zener model.